Dissolution of irregularly-shaped drug particles: mathematical modelling

M. Abrami [a], M. Grassi [a,*], D. Masiello [c], G. Pontrelli [b]

[a] Dept. of Engineering and Architecture, Trieste University, Via Alfonso Valerio, 6/A, Trieste I-34127, Italy
[b] Istituto per le Applicazioni del Calcolo - CNR, Via dei Taurini 19, 00185 Roma, Italy
[c] University of Edinburgh, The School of Engineering, R. Stevenson Road, Edinburgh EH9 3FB, UK

ARTICLE INFO

Keywords:
Dissolution
Irregular particles
Recrystallization
Wettability
Mathematical modelling

ABSTRACT

The prediction of drug dissolution profiles is crucial for elucidating the pharmacokinetic behaviour of drugs and the bioavailability of dosage forms. In this work, we develop a mathematical model to describe the dissolution process of irregularly shaped particles. We use a complete dissolution model that accounts for both surface kinetics and convective diffusion. The mechanistic relationship between the mass transfer coefficient and the local curvature is derived from the fundamental physical laws governing these processes. Our model theoretically shows that the dissolution rate depends nonlinearly on the surface curvature. The subsequent recrystallization process in the bulk fluid is also considered. The main result of this work is its simplicity, since only two coupled nonlinear ordinary differential equations are needed to describe the dissolution process. Another remarkable advantage is the possibility to determine the model parameters using common independent techniques, so that the importance of the wettability of solids on the dissolution process can be evaluated. Finally, the proposed model demonstrated the importance of particle shape in describing the experimental dissolution data of theophylline monohydrate.

1. Introduction

The dissolution of drugs means the detachment of molecules from the solid phase and their transport into the liquid phase surrounding the solid particle. Therefore, dissolution, which can only occur when the drug concentration in the liquid phase (solution) is lower than the solubility, should not be confused with the overall process of drug release from a delivery system, which typically involves other phenomena that may include dissolution [1]. According to Siepmann, drug dissolution can be defined as "the mixing of two phases (the solid and the liquid) with the formation of a new homogeneous phase (i.e., the solution)" [2]. The analysis of the dissolution phenomenon is not only interesting in itself, but also has important implications for the pharmaceutical field as it affects the bioavailability of drugs, i.e., the rate and extent to which the drug is absorbed from a delivery system and thus becomes available at the site of drug action [3,4]. As shown by the Biopharmaceutics Classification System [5], bioavailability depends on the permeability of the drug through the cell membrane and the dissolution of the drug in physiological fluids. The last aspect is absolutely relevant considering that about 40% of drugs on the market and 70–90% of new chemical entities have slow dissolution kinetics due to their poor water solubility [6-9]. These drugs include nonsteroidal anti-inflammatory drugs (NSAIDs), cholesterol-lowering drugs, antifungals, antibiotics, anticonvulsants, chemotherapeutics, antivirals, β-blockers, calcium channels, and immune-suppressants [10-15].

These considerations highlight the central role that drug dissolution plays in the pharmaceutical field and the need to fully understand the mechanisms that govern it in order to overcome practical problems and achieve optimal design of delivery systems. The need for rational approaches has also been promoted, for example, by the US Food and Drug Administration, which introduced and defined the concept of process analytical technology (PAT) as a mechanism for designing, analysing, and controlling pharmaceutical manufacturing processes by measuring critical process parameters that affect critical quality attributes [16]. Interestingly, PAT is not the only evidence of rational approaches in the pharmaceutical field, as, for example, the Quality by Design (QbD) strategy supports the same philosophy. According to the European Medicines Agency guidelines ICH Q8, QbD is defined as "a systematic development approach that starts with predefined objectives and emphasizes product and process understanding and control, based on sound science and quality risk management" [17]. The basic quantitative element of quantitative systems pharmacology (QSP) requires

* Corresponding author.
E-mail address: mario.grassi@dia.units.it (M. Grassi).

Accepted 24 June 2022

Fig. 1. Shape modification of a sugar grain upon dissolution in water at different times. Adapted from [42].

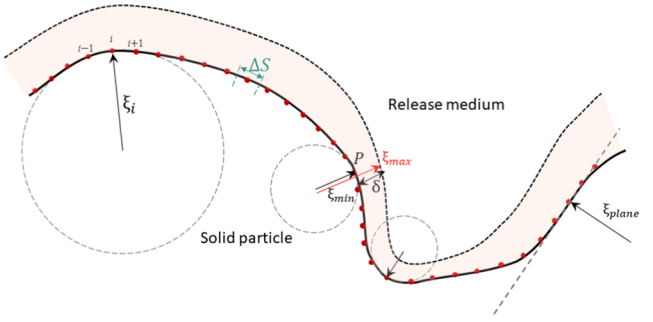

Fig. 2. Portion of a surface of a solid particle (2D case). The dashed circles are the local osculating circles in proximity of points *P* of the surface (solid line). The colored region represents the BL of thickness δ around the body surface where Fick's second equation is solved. Note that the BL thickness ($\delta = D/k_d$) depends on the local curvature. The white region represents the solid particle (below) and the external bulk fluid (above) (figure not to scale).

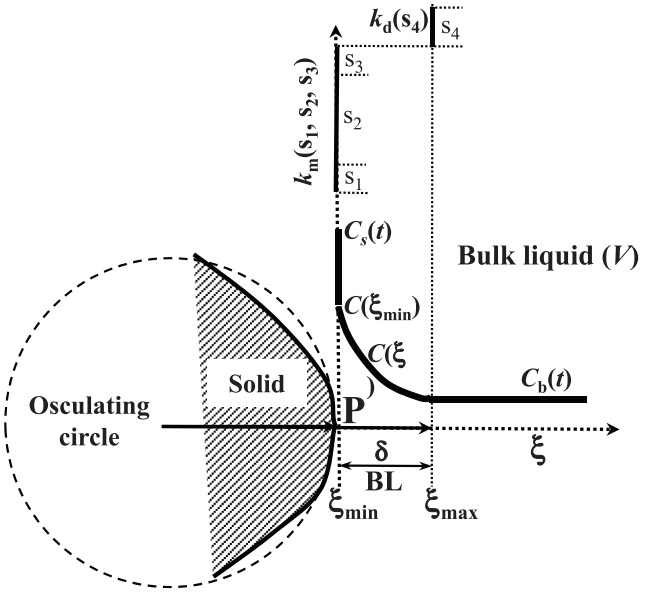

Fig. 3. Spatial disposition of the different model parameters corresponding to the generic surface point "P" depicted in Fig. 2. C_b is the bulk drug concentration, C_0 (=$C(\xi_{min})$) is the solid–liquid interface drug concentration, C_s indicates drug solubility, k_d is the *hydrodynamic* mass transfer coefficient (depending on dissolution steps s_1, s_2 and s_3) while k_m is the *interface* mass transfer coefficient (depending on dissolution step s_4).

mathematical models that aim to describe biological systems and mimic their responses to internal stimuli, environmental factors, and drug delivery [18].

This framework explains the current demand of increasingly sophisticated mathematical models capable of interpreting experimental evidence. In the particular case of dissolution of solid particles in water or in a physiological fluid [19,20], mathematical models considered

Table 1
Physical parameters used to simulate the dissolution of a theophylline particle characterized by different shapes (circle, ellipse, and corrugated circle) with the same initial volume [10,50]. The dimensionless volume of the release medium (V^+) is calculated as the ratio between the volume of the release medium and the initial particle volume (V_0).

Parameter	unit	Value
Initial particle mass: M_0	kg	$7.8{\cdot}10^{-10}$
Initial particle volume: V_0	m^3	$5.23{\cdot}10^{-13}$
Solid drug density: ρ_s	kg/m^3	1490
Initial drug solubility (25° C): C_{s0}	kg/m^3	11.6
Final drug solubility (25° C): C_{sf}	kg/m^3	6.1
Surface recrystallization constant: k_r	s^{-1}	$6{\cdot}10^{-3}$
Bulk recrystallization constant: k_{rb}	s^{-1}	$6.6{\cdot}10^{-3}$
Interface mass transfer coefficient: k_m	m/s	$3.7{\cdot}10^{-3}$
Drug diffusivity in water (25 °C): D	m^2 /s	$6.2{\cdot}10^{-10}$
Fluid density: ρ_f	kg/m^3	1000
Fluid dynamic viscosity: η_f	Pa s	10^{-3}
Dimensionless release medium volume: V^+	–	150 and 300
Exponent for concave surfaces: n	–	0.49

some potentially important aspects such as the wettability of the drug, the hydrodynamic conditions of the dissolution medium, the possible change in solubility due to the phase transition during dissolution, the shape of the particles, the size distribution of the particles, and a finite dissolution volume. Historically, the first fundamental approach to describe the dissolution of particles was that of Hixson and Crowell [21-23], who for the first time considered the surface reduction in the dissolution of spherical particles and established the well-known cubic law. Later, the elegant model of Pedersen and coworkers also considered the size distribution of spherical particles [24-27]. Interestingly, this model can be reduced to the Hixson-Crowell model in the case of monodisperse spherical particles. Since then, many other models have been developed to improve the theoretical description of particles dissolution. For example, mathematical modelers focused on the solid–liquid interface by arguing that the overall dissolution process can be affected either by limited wettability of the solid [10] or by the occurrence of an interfacial reaction between solute and solvent molecules [28-30]. In either cases, the end result is a time-dependent drug concentration at the solid–liquid interface that is different from the solubility of the drug in the solvent.

A topic closely related to this aspect concerns metastable solids that undergo a phase change (amorphous-crystalline or polymorphic transformation) upon dissolution [31,32]. Other research indicated that the drug concentration profile in the boundary layer (BL) surrounding the solid surface is not linear, as originally assumed [33-35], unless dissolution occurs from a flat surface. This aspect is very important because the thickness of BL is also affected by the hydrodynamic conditions of the fluid environment [28]. Although some authors question the reliability of this statement [36], other researchers have developed a very interesting and simple approach to evaluate the BL thickness dependence on hydrodynamic conditions [37,38]. Interestingly, for a comprehensive description of drug dissolution, the possible drug degradation in the bulk fluid after dissolution [39] and the effects of a finite fluid environment were also considered. Another parameter attracted the interest of researchers, namely the shape of the dissolving

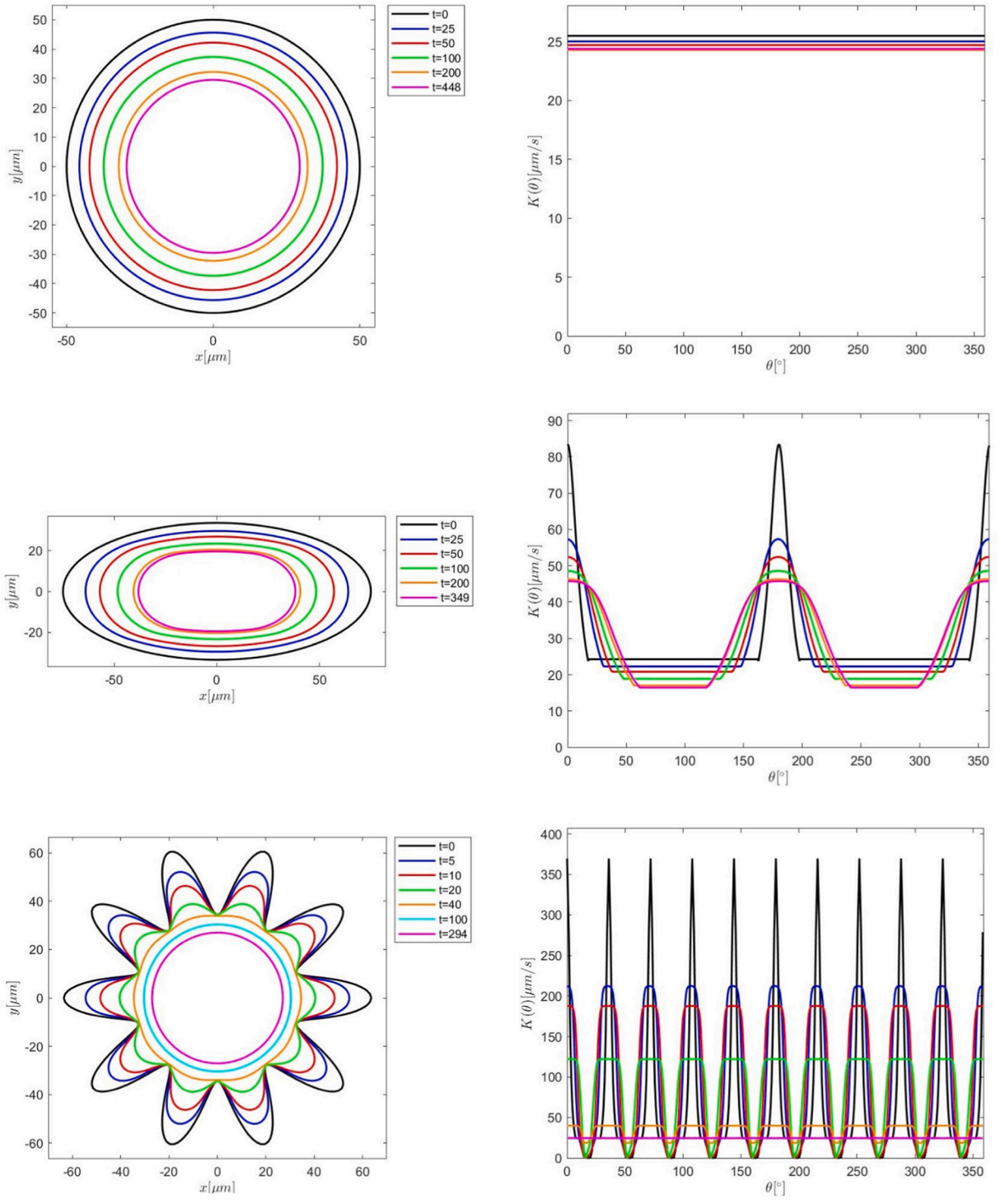

Fig. 4. Time evolution of the shape (left) and overall mass transfer coefficient K (right) as a function of the angle θ (right) for a circle, ellipse and corrugated circle during dissolution (V^+=150). In each row, equal colors correspond to equal times, with black line as initial time.

particles [40]. While Hirai and co-workers did not explicitly consider the shape of the particles but focused on a law that can describe the time dependence of the dissolution surface [41], Abrami et al [32] dealt with spherical, cylindrical and parallelepiped particles. Although some authors have focused on the dissolution of irregularly shaped particles [42], to the best of our knowledge, no comprehensive mathematical study taking into account both the particle shape and the above-mentioned aspects of dissolution has been carried out. In practise, it is indeed important to know which of the different aspects determining dissolution plays the most important role, depending on the solid and the dissolution conditions considered. For example, regarding the particle shape, it is known [40] that the shape can affect the dissolution since it is related to the thickness of the particles BL. Moreover, it is known that the convex parts of the particle surface tend to dissolve faster than flat surfaces, resulting in rounded edges and corners, as shown in Fig. 1 in the case of dissolution of sugar grains [42]. Similar findings apply to the dissolution of succinic acid grains [43].

Thus, the objective of this work is to develop a mathematical model

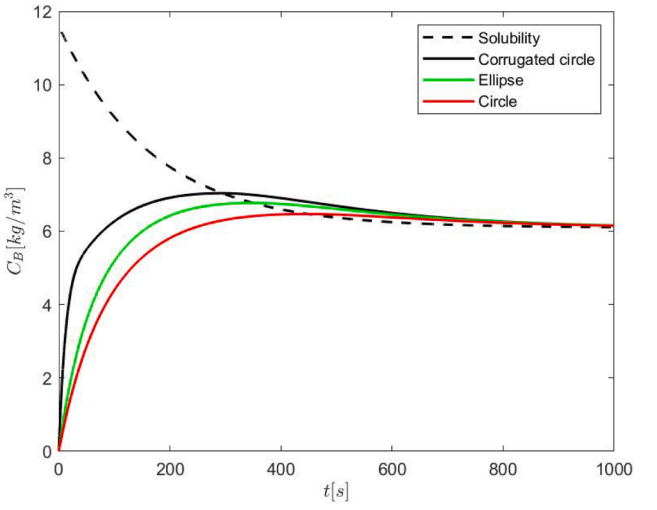

Fig. 5. Change in theophylline bulk concentration (C_b) with time in the three cases circle, ellipse, and corrugated circle (V^+=150). The dashed line shows the solubility curve. It can be seen that the corrugated circle dissolves much faster than the other two shapes, with a higher concentration in the release medium.

capable of relating the effect of particle shape to the main phenomena governing particle dissolution, such as the wettability of the solid, the change in drug phase (and solubility) upon dissolution, the diffusion of the drug inside BL, the effect of surface curvature and hydrodynamics on thickness BL, and the presence of a finite release environment. To generalize the simulation results and facilitate comparison with conventional shapes, the volume and surface shape coefficients are evaluated for each geometry considered [44].

2. Mathematical modelling of drug dissolution

Dissolution can be considered as a process consisting of five simultaneous phases [2,35,45]:

1) contact of the solvent with the solid surface (wetting), which implies the formation of a solid–liquid interface, starting from a solid–vapor interface,
2) breaking of intermolecular bonds in the solid phase (fusion),
3) Transfer of molecules from the solid phase to the solid–liquid interface (solvation),
4) Diffusion of solvated molecules through the immobile BL, surrounding the solid surface (diffusion),
5) Convective transport of the solvated drug molecules into the well-stirred bulk solution (convection).

While step 5) is the less interesting one, as it simply depends on the Reynolds number in the dissolution fluid, the first four are the classical target of mathematical models used to describe particle dissolution. In fact, the first four steps can be considered as the sum of four energy contributions representing the total resistance that the drug molecules must overcome to pass from the solid phase to the dissolved phase (dissolution). Clearly, the higher the dissolution energy required (i.e., the higher the mass transfer resistance), the lower the dissolution kinetics. Interestingly, as discussed below, particle shape mainly affects step 4).

To characterize the first four steps, we need to know the time evolution of the drug concentration profile in the immobile stagnant BL, surrounding the solid surface S. Indeed, BL is unavoidable and its thickness depends on 1) the relative velocity between the solid surface and the external fluid, 2) the kinematic fluid viscosity, and 3) the drug diffusion coefficient within BL [37]. Under suitable boundary conditions (see Appendix), the analytical solution of the so-called second Fick's

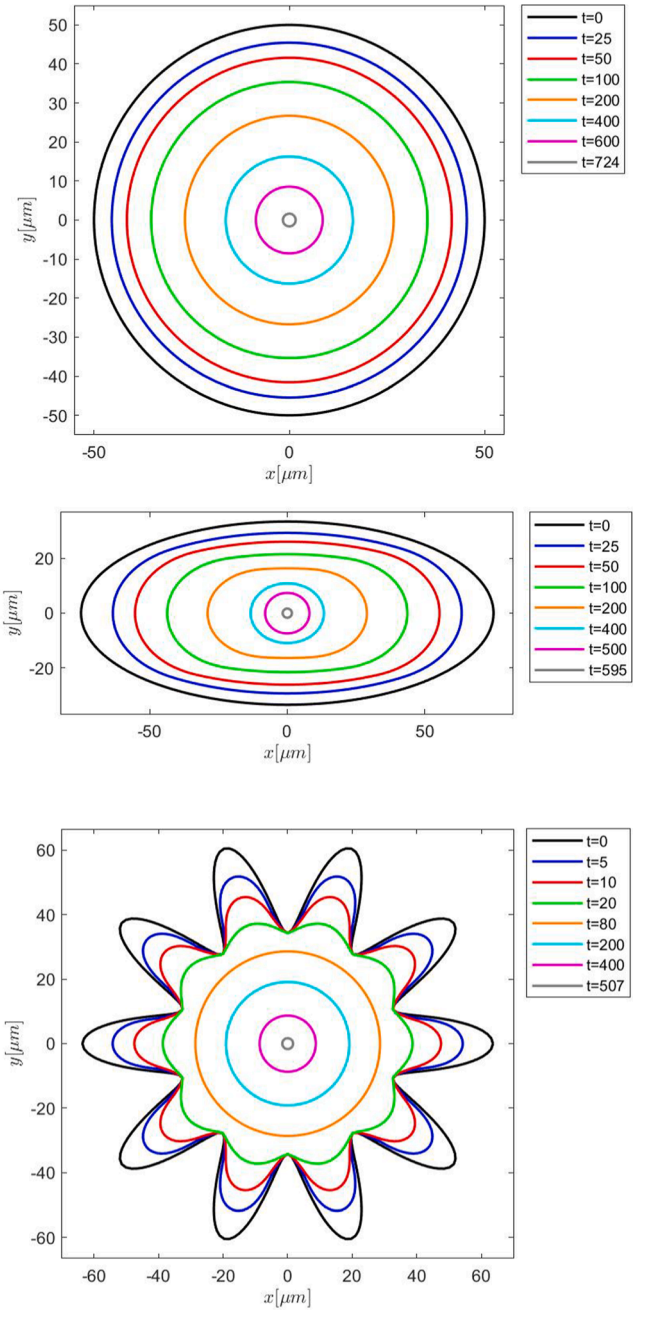

Fig. 6. Temporal evolution for circle, ellipse and corrugated circle until complete dissolution (V^+=300). The rounding of the shape is more evident, with the dissolution of the particles occurring at different times (cfr. Fig. 4).

second equation related to the surface point P (see Fig. 2), assuming pseudo stationary conditions and spherical coordinates (i.e. local radial coordinate), allows us to conclude that the drug profile concentration ($C(\xi)$) is not linear and is [32]:

$$C(\xi) = C_b + (C_s - C_b)\frac{k_m}{k_d}\xi_{min}^2\left(\frac{\xi_{max}}{\xi} - 1\right)\Big/\left(\delta\left(\xi_{max} + \frac{k_m}{k_d}\xi_{min}\right)\right) \quad (1)$$

where C_b is the drug concentration in the bulk liquid (see Fig. 3), C_s is the drug solubility, and $\delta(P)$ is the local BL thickness. k_d (m/s) is the hydrodynamic mass transfer coefficient, which is the ratio between the drug diffusion coefficient (D) in BL and δ ($k_d = D/\delta$). While k_d, also called the intrinsic dissolution constant, takes into account dissolution step 4, k_m (m/s) is the interfacial mass transfer coefficient, which

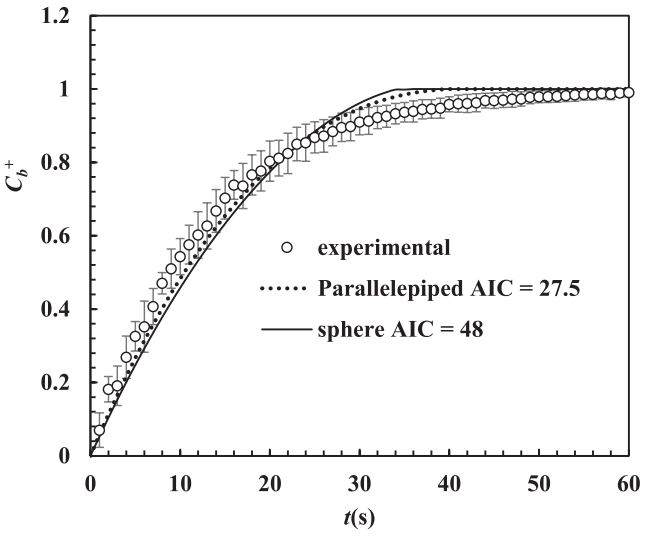

Fig. 7. Best fit of the model (solid and dotted lines) to experimental data (white circles) related to dissolution of TMH particles. C_b^+ indicates the ratio between the drug concentration in the dissolution environment (C_b) at time t and after a very long time. Model fitting was performed assuming spherical (solid line) or parallelepipedal crystals (dotted line). The vertical bars indicate the standard deviation, while *AIC* is the Akaike number (Eq. 11)).

depends mainly on the wetting properties of the dissolution surface (step 1). Finally, ξ_{min} represents the radius of the osculating circle that approximates the real surface profile near P, while ξ_{max} is equal to the sum of δ and ξ_{min} (see Fig. 2).

Although k_m depends in principle on the local radius of curvature (ξ_{min}), for practical purposes it can be retained constant with ξ_{min} (see Appendix). In general, however, k_m should depend on position because of surface anisotropies arising from possible different orientations of surface molecules belonging to different crystal faces. These surface anisotropies can affect the dissolution steps 1) and 2) by changing the local melting temperature/hentalpy [46] and the local surface wettability [47], which in turn affects the variation of k_m. However in the following, for simplicity, k_m is considered independent of time and location. In contrast, the dependence of k_d on ξ_{min} is not negligible, and its evaluation can be done according to the approach followed by D'Arcy and Persoons [37]. This strategy relies on the equation of Ranz and Marshall, which was originally developed to describe the evaporation rate of pure liquid droplets [48,49] and then used to simulate the mass transfer of solid spheres under forced convection [20]:

$$k_d = \frac{D}{2\xi_{min}}\left(2 + 0.6\sqrt{\frac{\Delta U \cdot 2\xi_{min}}{\nu_f}}\left(\frac{\nu_f}{D}\right)^{\frac{1}{3}}\right) \tag{2}$$

where ν_f is the fluid cinematic viscosity and ΔU is the relative solid particle-liquid velocity that can be approximated by [37]:

$$\Delta U \approx (\rho_s - \rho_f) g \frac{(2R)^2}{18\eta_f} \tag{3}$$

where ρ_s and ρ_f are the density of the solid and liquid, respectively, g is the gravity acceleration, η_f is the dynamic viscosity, and R is the radius of an "equivalent" sphere with the same particle volume. Since ξ_{min} varies with position, Eq. (2) states that k_d is position dependent and decreases with ξ_{min}. Since all other dissolution parameters are constant, this leads to the well-known faster dissolution of peaks and spikes (very small local radius of curvature) compared to a flat surface corresponding to an infinite radius of curvature [42,43].

Since in the case of irregularly shaped particles there is a need to describe the dissolution of solids from flat and concave surfaces, we also assume suitable dissolution equations for these types of solid surfaces. For a flat surface, we resort to the Levich approach [50], which was developed for modelling the dissolution of a rotating flat surface, where the rotational velocity is replaced by $\Delta U/R$:

$$k_d = 0.621 D^{2/3} \nu_f^{-1/6} \sqrt{\frac{\Delta U}{R}} \approx 0.621 D^{2/3} \nu_f^{-1/6} \sqrt{(\rho_s - \rho_f) g \frac{2R}{9\eta_f}} \tag{4}$$

In the absence of theoretical approaches to describe the dissolution of solid drugs from concave surfaces, we have adopted the following empirical equation:

$$k_d = k_{d-plane}\left(\frac{\xi_{min}}{\xi_{plane}}\right)^n \tag{5}$$

where n is a model parameter. Basically, Eq. (5) assumes that, unlike convex surfaces, the dissolution kinetics of a concave surface decreases with its curvature radius ξ_{min} because the relative velocity ΔU between the surface and the fluid decreases locally as ξ_{min} decreases. In summary, eqs. (2), (4), and (5) allow us to determine the correct k_d value when moving with continuity from convex to flat or concave to flat surfaces characterized by different radii of curvature ξ_{min}. Referring to the definition of k_d (=D/δ), our approach implies that the thickness of BL on an irregular surface is position dependent and increases with ξ_{min} to a flat surface in the case of a convex surface (see Appendix). Conversely, in the case of a concave surface, starting from a flat surface, δ decreases with ξ_{min}.

To evaluate the amount of drug dissolved (M_b) by time t, we used the total drug mass balance, which states that the change in M_b over time (dM_b/dt) must equal the drug flux leaving the solid dissolving surface S (derivative of Eq (1) with respect to ξ):

$$\frac{dM_b}{dt} = V\frac{dC_b}{dt} = -S\left(D\frac{\partial C}{\partial \xi}\right)\Big|_{\xi=\xi_{max}} = SK(C_s - C_b) \tag{6}$$

where V is the bulk liquid volume (supposed constant) and K (m/s) is the *overall* mass transfer coefficient [32]:

$$K = \frac{\xi_{min}/\xi_{max}}{\frac{1}{k_d} + \frac{1}{k_m}\frac{\xi_{max}}{\xi_{min}}} \tag{7}$$

Since we are dealing with irregularly shaped particles, k_d and hence K are location dependent (see Eqs. (2) and (5)). Consequently, the description of the whole dissolution phenomenon requires the subdivision of S into elementary surfaces ΔS_i (see Fig. 2) and the determination of the local osculating circle radius. This, in turn, allows the calculation of M_b and the change of particle shape in the course of dissolution (see Appendix).

To complete the model, it is necessary to evaluate both C_s and C_b. As mentioned in the introduction, it is quite common for the drug to undergo a phase transformation (polymorphic or amorphous-crystalline) upon dissolution, resulting in a decrease in solubility. This phenomenon is usually described by a first-order reaction [51] occurring at the solid–liquid interface, leading to the following expression for the reduction of C_s over time:

$$C_s(t) = C_{sf} + (C_{s0} - C_{sf})e^{-k_r t} \tag{8}$$

where C_{sf} and C_{s0} are the final and initial solubility values, respectively, while k_r is the recrystallization constant. In fact, Eq. (8) accounts for the dissolution step 2), since the solubility is directly related to the decay behaviour of the crystal network, which is quantified by its melting temperature and enthalpy [46]. Of course, more complex models describing the phase and solubility time variations (nucleation and growth approach or de-nucleation approach [52]) could have been considered. However, due to its simplicity and reliability, Eq. (8) was used to model the solubility-time variation due to a surface phase transition induced by contact with a liquid phase [11,41,51].

To evaluate C_b and close the balance between unknowns and

equations, the total mass balance of the drug can be considered:

$$M_0 = \sum_i M_s^i + VC_b(t) + M_c(t) \tag{9}$$

Eq. (9) states that at each time the sum of the undissolved ($\sum_i M_s^i$), dissolved (VC_b), and recrystallized (within the dissolution environment) drug mass (M_c) is equal to the original drug mass M_0. Although more complex approaches could be considered [53], we opted for a simple first-order approach to model the temporal evolution of M_c:

$$\frac{dM_c}{dt} = -k_{rb}\, V(C_s(t) - C_b(t)) \qquad C_b(t) \geq C_s(t) \tag{10}$$

where k_{rb} is the bulk recrystallization constant. It is clear that recrystallization can occur only when the mass concentration (C_b) exceeds the time-dependent solubility $C_s(t)$. Similarly, dissolution can occur under the condition that $C_b < C_s$.

3. Materials and methods

Theophylline monohydrate (TMH) (Carlo Erba, Milan. Italy; $C_7H_8N_4O_2{\cdot}H_2O$, $MW = 198.2$, $\rho = 1.49$ g/cm^3) was used as model drug. Dissolution tests were performed by rapidly pouring a known amount of drug (3 mg) into 150 cm^3 of distilled water placed inside a double-walled beaker sealed with a lid (inner cell diameter = 5 cm; height = 10 cm). The temperature was kept constant (37 °C) by a liquid (water) flowing between the inner and outer walls of the cell and coming from the thermostat unit. A magnetic stirrer (length = 2.5 cm) placed at the bottom of the inner cylinder and rotating at 200 rpm ensured good mixing of the dissolution medium ($Re > 10^4$). The TMH concentration in the dissolution medium environment was determined using an optical fiber apparatus (HELLMA, Milano, Italy) connected to a spectrophotometer (ZEISS, Oberkochen, Germany) and controlled by a user interface (Aspect Plus, Carl-Zeiss Oberkochen, Germany). The measurement probe, which was connected to the last part of the optical fiber, was inserted into the dissolution medium through a small hole that crossed the cell lid. To avoid possible noise due to the presence of undissolved drug particles flowing in the dissolution medium, the absorbance measured at 272 nm was subtracted by the absorbance measured at 500 nm (i.e. very far from TMH absorbance peak (272 nm)), since noise due to particles scattering is almost independent of wavelength. The dissolution tests were performed in triplicate.

Models comparison was performed recurring to the Akaike's Information Criterion (*AIC*) [54]:

$$AIC = N_s \ln\left(\frac{\chi^2}{N_s}\right) + 2\frac{(M+1)N_s}{N_s - M - 2} \tag{11}$$

where N_s is the number of experimental data, M is the number of fitting parameters, and 2 is the sum of squared differences between experimental data and model averaged over data variance. The model with a smaller *AIC* must be preferred.

4. Results and discussion

The model was solved computationally for a variety of particles with different shapes and curvature ranges. Particle shape is an inherent feature that plays an important role in dissolution kinetics and has been extensively studied in sedimentary rock geology and morphology [55,56]. In particular, sphericity and roundness are two simple and useful dimensionless numbers that measure various morphological properties such as deviation from spherical shapes [44].

Sphericity (*SP*) is a measure of the degree to which a particle approximates the shape of a sphere and is independent of its size. There are several definitions [57,58], but the most practical and effective is the ratio between the radii of the inscribed (R_I) and circumscribed (R_c) sphere:

$$SP = \frac{R_I}{R_c} \tag{12}$$

Roundness (*RG*) quantifies the sharpness of particle corners (in a number N) as the ratio of the average radius of curvature of the edges or corners r_k to the radius of the maximum incircle R_I [57]. For our purposes, this is measured as:

$$RG = \frac{1}{N}\sum_{k=1}^{N}\frac{r_k}{R_I} \tag{13}$$

While $SP = RG = 1$ for a sphere, values of SP and $RG \ll 1$ indicate a great departure from spherical shape, and therefore a very irregular form.

We limit ourselves here to three case studies of shapes with a well-defined structure, representative of many others: the circle ($SP = RG = 1$), the ellipse (ratio of axes: 2.25, $SP = RG = 0.44$), and the corrugated circle (amplitude of corrugation/radius: 0.3, number of corrugations: 10, $SP = 0.53$, $RG = 0.04$). The dissolution curves and the concentration evolution of a single particle (or an ensemble of identical particles) with different shapes but the same initial volume (and the same drug concentration) are calculated and compared. Although our simulation is limited to the two-dimensional case, most dissolving particles can be approximated as rotating bodies about the axis perpendicular to the plane of greatest stability, and the conclusions of 3D dissolution can be easily carried over from our case by projection. Therefore, the terms volume (area) and surface (line) will be used equally in the following.

A MATLAB routine was developed to implement the algorithm described in Section 2 and a typical number of 400 points is used to discretize the boundary line.

To evaluate the potential of the model, we focused on a very common drug in the pharmaceutical field, namely TMH. This drug, often used as a model drug because it is cheap, safe, and easily detectable in solution with UV light is an essentially neutral compound with bronchodilator activity. For this reason, it is used to treat asthma, bronchospasm, and chronic obstructive pulmonary disease. Because its water contact angle is about 72° (work of immersion at 25 °C − 0.0223 J/m^2), it can be considered moderately water-wettable if compared with a water-wettable drug such as griseofulvin (antifungal, $C_{17}H_{17}ClO_6$, water contact angle 52°, work of immersion at 25 °C − 0.0431 J/m^2) and a not so well wettable drug like nimesulide (NSAID, $C_{13}H_{12}N_2O_5S$, water contact angle 92°, work of immersion at 25 °C − 0.0024 J/m^2) [10]. Interestingly, the anhydrous form of theophylline ($C_7H_8N_4O_2$, $M_w = 180.2$) transforms into the more stable monohydrate form upon dissolution in water [59]. This polymorphic transformation leads to a decrease in solubility (T = 25 °C and pH = 7) from $C_{s0} = 11.6$ kg/m^3 (anhydrous) to $C_{sf} = 6.1$ kg/m^3 (monohydrate). Moreover, the diffusion coefficient of TMH in water at 25 °C is $D = 6.2{\cdot}10^{-10}$ m^2/s, while the recrystallization constant at the surface is $k_r = 6{\cdot}10^{-3}$ s^{-1} and $k_m \sim 3.7{\cdot}10^{-3}$ m/s [10]. It is worth noting that k_m and k_d are of the same order of magnitude for theophylline, so the mass transfer resistance is comparable in magnitude due to wettability ($1/k_m$) and hydrodynamic ($1/k_d$) coefficients.

The above discussion makes clear why we based our simulations on TMH. Indeed, the dissolution of this drug can in principle be influenced by wettability, hydrodynamics, recrystallization, and shape. To complete the scenario, we also considered two different situations in terms of the dimensionless volume of the release medium (V^+, defined as the ratio between release medium and particle volume), a very important parameter in the experimental design of particle dissolution. Two values for V^+ (150, 300) were selected. Setting $V^+ = 150$ implies a theoretical final drug concentration in the release medium that exceeds the solubility of TMH ($C_{sf} = 6.1$ kg/m^3), so recrystallization is expected during dissolution. On the other hand, $V^+ = 300$ results in a final drug concentration far below the solubility of TMH, so recrystallization cannot occur because the release environment medium is too large relative to the particle volume. Table 1 summarizes all parameter values

considered for model simulations assuming theophylline particles.

Fig. 4 (left) shows the time evolution of the particle surface in the case of a circle, an ellipse, and corrugated circle, respectively, assuming $V^+ = 150$. Interestingly, both the ellipse and the corrugated circle tend to assume a round shape with time, which is consistent with the experimental results in Fig. 1. The higher k_d value (Eq. (2)) (and hence the higher K value, see Eq. (7)) corresponding to convex surface sections characterized by a smaller local radius of curvature implies faster local dissolution leading to the elimination of local peaks. This interpretation is supported by the time and angular position dependence (θ) of the total mass transfer coefficient K in Fig. 4 (right). It can be seen that K increases in the case of both the ellipse and the corrugated circle in correspondence with the sharper points and attenuates as time progresses.

Fig. 5 shows the macroscopic effect of what is shown in Fig. 4, i.e., the time evolution of theophylline concentration (C_b) in the release environment with respect to round, elliptical, and corrugated particles. It can be seen that regardless of the particle shape, recrystallization starts when all the bulk concentration curves (colored lines) cross the decreasing solubility of the drug (black dashed line). Moreover, it is obvious that the initial particle shape plays an important role, since the dissolution rate increases with the degree of irregularity of the particles, in particular with the index RG: corrugated circle ($SP = 0.53$, $RG = 0.04$) dissolves faster than an ellipse ($SP = RG = 0.44$), which in turn dissolves faster than a sphere ($SP = RG = 1$).

Finally, Fig. 6 shows the results of a simulation in which a larger volume of the release medium (300 times that of the particles) was assumed. In this case, no recrystallization occurs in the bulk fluid due to the low C_b values, and the particle shape plays the predominant role. As in Fig. 5, more irregular shapes lead to a faster dissolution rate than the sphere (circle), which is the most regular shape.

In order to finally prove the importance of particle shape on drug dissolution, our model was fitted twice to experimental data referring to TMH dissolution. In the first case spherical (unrealistic) drug particles were considered while, in the second case, squared base parallelepid drug particles (much more realistic: parallelepiped length was set 4 times the base side. see Fig. 4 of [32]) were considered. As fitting parameter we assumed a characteristic length of the particles. In the case of spherical particles, it was the average radius, while the radius of the equivalent sphere (i.e. the sphere sharing the same volume with the average parallelepiped) was considered in the case of parallelepiped. All other model parameters were: $\rho_s = 1490$ kg/m^3, $T = 37$ °C, $k_r = k_{rb} = 0$, $C_{s0} = C_{sf} = 12.495$ kg/m^3, $\mu_f = 6.91 \cdot 10^{-4}$ Pa s and $\rho_f = 993$ kg/m^3 [10]. Fitting outcomes (see Fig. 7) revealed that data description is better (lower AIC ($N_s = 60$, $M = 1$)) when the more relasitic parallelelpiped drug particle was considered. Moreover, the characteristic length in the case of the sphere and the ashlar was 18 and 21 μm, respectively. Obviously, the discrepancy between model best fit and the experimental data is due to the assumed mono-dispersity of the particle size.

5. Conclusions

The numerical results show the role and importance of local surface curvature and particle shape on the drug dissolution kinetics and demonstrate how they correlate with the release rate, even nonlinearly. The simulation results are supported by experimental evidence of crystal shape change upon dissolution and by fitting the model to experimental data. The proposed model thus provides a new understanding of drug mass transfer and the influence of various parameters, such as particle shape, on the mechanism of drug dissolution. Consequently, by demonstrating the correlation between material transport properties and numerous variables, our model can be used to find and optimize the processing parameters that determine the *in vivo* dissolution of solid particles, a phenomenon that affects drug bioavailability. The model can be readily extended to three-dimensional cases of solid particles rotating about the axis of symmetry and, with additional computational effort, to more complex 3D particles. It is worth noting that simpler models of the dissolution phenomenon failed in describing our simulation results, further emphasizing the need for more complex models when attempting to reliably describe/interpret dissolution experiments.

Our results indicate the possibility of designing the shape of drug particles to ensure a desired dissolution rate and such that the concentration reaches a certain value in a certain time. Thus, the present model provides useful support for the development of suitable particles to achieve a therapeutic release rate by applying a systematic strategy with a limited number of experiments.

Declaration of Competing Interest

The authors declare that they have no known competing financial interests or personal relationships that could have appeared to influence the work reported in this paper.

Acknowledgement

Funding from the European Research Council under the European Unions Horizon 2020 Framework Programme (No. FP/2014–2020)/ERC Grant Agreement No. 739964 (COPMAT) is acknowledged.

Appendix

In this section, additional details are given on the derivation of the curvature-dependent relations and on the mechanistic equations used in Section 2. To obtain the time evolution of the drug concentration profile in the unstirred stagnant BL around the solid surface S, we used the so-called second Fick's second equation:

$$\frac{\partial C}{\partial t} = \nabla(D \nabla C) \tag{A.1}$$

where C is drug concentration, t is time, D is the drug diffusion coefficient in BL while ∇ is the gradient. The first model assumption is based on the hypothesis that mass transport inside BL is one-dimensional and occurs in the direction $\boldsymbol{n}$ perpendicular to the solid surface S. The second is that pseudostationary conditions are rapidly reached in BL. Assuming sink conditions and planar, cylindrical or spherical particles, Tseng and co-workers [60] have presented a very interesting approach aimed at verifying whether the pseudostationary assumption holds in the interior of BL. When sink conditions are not attained, the numerical solution of Eq. (A.1) shows that the pseudostationary conditions are physically correct when the usual values for D ($\sim 10^{-10}$ m^2 s^{-1}) [10] and the thickness of BL ≤ 20 μm are assumed. Thus, Eq. (A.1) becomes:

$$\nabla(D \nabla C) = 0 \tag{A.2}$$

Eq. (A.2) must be solved in one dimension in the vicinity of a point P on the surface S, where the solid is approximated by a local osculating circle of radius min (Fig. 2). Eq. (A.2) requires the following initial and boundary conditions:

$$C(\xi) = 0 \qquad \xi_{min} < \xi \leq \xi_{max} \tag{A.3}$$

Boundary:

$$(D\nabla C{\cdot}n)\,|_{\xi=\xi_{min}} = -k_m(C_s - C(\xi_{min}))\tag{A.4}$$

$$C(\xi_{max}) = C_b \tag{A.5}$$

where ξ is the local one dimensional spatial coordinate, $\delta = \xi_{max} - \xi_{min}$ is the thickness of BL, C_s is drug solubility in the dissolution liquid, C_b is the drug concentration in the dissolution medium while k_m (m/s) is the *interface* mass transfer coefficient, mainly depending on the dissolution surface wetting properties. Eq. (A.3) states that BL does not contain drug molecules at the initial time, while Eq. (A.4) states that the drug flux leaving the solid surface depends on k_m and on the difference between the solubility of the drug and the drug concentration at the solid surface on the liquid side. Finally, Eq. (A.5) states that the drug concentration at the BL - bulk liquid interface is equal to C_b.

The analytical solution of Eq. (A.2)-(A.5), which refers to the point P of the surface (see Fig. 2), is given by Eq. (2) [32]:

$$C(\xi) = C_b + (C_s - C_b)\frac{k_m}{k_d}\xi_{min}^2\left(\frac{\xi_{max}}{\xi} - 1\right)/(\delta(\xi_{max} + \frac{k_m}{k_d}\xi_{min})) \tag{1}$$

where k_d (m/s) is the *hydrodynamic* mass transfer coefficient ($=D/\delta$). In addition, Eq. (1) allows evaluating the drug concentration C_0 in $\xi = \xi_{min}$, i.e., at the solid–liquid interface (liquid side):

$$C_0 = C_b + (C_s - C_b)\frac{\xi_{min}}{\frac{k_d}{k_m}\xi_{max} + \xi_{min}} \tag{A.6}$$

Eq. (A.6) states that at $t = 0$, when $C_b = 0$, C_0 is a fraction of C_s, while $C_0 = C_s$ after a very long time when $C_b = C_s$, i.e. C_0 increases with time up to C_s. In the two limiting cases, when $k_m \to \infty$, (high wettability or hydrophilic surface) $C_0 \to C_s$, while, when $k_m \to 0$ (very poor wettability or hydrophobicity), $C_b = 0$. Obviously, Eq. (1) requires the determination of the two mass transfer coefficients k_m and k_d. The starting point for k_m evaluation is the Tolmann equation [61]:

$$\gamma = \gamma^{\infty}\frac{\xi_{min}}{\xi_{min} + d_T} \tag{A.7}$$

where γ and γ^{∞} are, respectively, the specific surface tension (or specific surface energy) associated to a flat surface (infinite curvature radius) and a surface of curvature radius ξ_{min}, d_T is the Tolmann length whose order of magnitude should correspond to the diameter of the molecules constituting the curved surface [62], but it is usually assumed to be 1/3 of the molecules diameter [63]. Inserting Eq. (A.7) in the equation defining the work of immersion W_I, we get:

$$W_I = \gamma_{sl} - \gamma_{sv} = (\gamma_{sl}^{\infty} - \gamma_{sv}^{\infty})\frac{\xi_{min}}{\xi_{min} + 2d_T} \tag{A.8}$$

where γ_{sl} and γ_{sv} represent the solid–liquid and solid-vapour specific surface energies, respectively, competing with a curved surface, while γ_{sl}^{∞} and γ_{sv}^{∞} indicate the same specific surface energy, but refer to a flat surface. Based on Eq. (A.8) and the experimental results of Grassi et al [10], we can affirm:

$$k_m \propto \frac{1}{W_I - W_I^0} = \frac{1}{(\gamma_{sl}^{\infty} - \gamma_{sv}^{\infty}) - (\gamma_{sl}^{\infty} - \gamma_{sv}^{\infty})^0}\frac{\xi_{min} + 2d_T}{\xi_{min}} \tag{A.9}$$

where W_I^0 is the work of immersion when no wettability issues occurs (contact angle ≈ 0). Thus, Eq. (A.9) can be rewritten as:

$$k_m = k_m^{\infty}\frac{\xi_{min} + 2d_T}{\xi_{min}} \tag{A.10}$$

where k_m^{∞} represents the k_m value associated with a plane surface ($\xi_{min} \to \infty$). Although Eq. (A.10) predicts a curvature dependence of k_m, k_m is virtually curvature independent because of the very small values typically associated with d_T ($\leq$0.5 nm). The evaluation of k_d can be done according to the approach used by D'Arcy and Persoons [37]:

$$k_d = \frac{D}{2\xi_{min}}\left(2 + 0.6\sqrt{\frac{\Delta U{\cdot}2\xi_{min}}{\nu_f}}\left(\frac{\nu_f}{D}\right)^{\frac{1}{3}}\right) \tag{2}$$

where ν_f is the fluid cinematic viscosity and ΔU is the relative solid–liquid velocity that can be approximated by:

$$\Delta U \approx (\rho_s - \rho_f)g\frac{(2R)^2}{18\eta_f} \tag{3}$$

where ρ_s and ρ_f are the density of the solid and liquid, respectively, g is the gravity acceleration, η_f is the dynamic viscosity, and R is the radius of an "equivalent" sphere with the same particle volume. Since ξ_{min} varies with position, Eq. (2) states that k_d is position dependent and decreases with ξ_{min}. Since in the case of irregularly shaped particles there is a need to describe the dissolution of solids from flat and concave surfaces, we also assume suitable dissolution equations for these types of solid surfaces. For a flat surface, we resort to the Levich approach [50], which was developed for modelling the dissolution of a rotating flat surface, where the rotational velocity is replaced by $\Delta U/R$:

$$k_d = 0.621 D^{2/3} \nu_f^{-1/6} \sqrt{\frac{\Delta U}{R}} \approx 0.621 D^{2/3} \nu_f^{-1/6} \sqrt{(\rho_s - \rho_f) g \frac{2R}{9\eta_f}} \tag{4}$$

Fig. A.1 shows the comparison between Eq. (2) (solid line) and Eq. (5) (thick dashed line) assuming typical values for their parameters ($D = 5\ 10^{-10}$ m^2/s, $v_f = 10^{-6}$ m^2/s, $\eta_f = 10^{-3}$ Pa·s, $\rho_s = 1500$ kg/m^3 and $\rho_f = 1000$ kg/m^3, $R = 5{\cdot}10^{-4}$ m) [10]. It can be seen that for $\xi_{min} \approx 244$ m, the two equations provide the same k_d estimate, and for larger values of min, the difference between the two equations is relatively small (<37% to $\xi_{min} = 600$ μm). Thus, we can identify the radius plane, which represents the transition from a convex to a plane surface, with the value ξ_{min} corresponding to the intersection of Eq. (2) and Eq. (A.11) (244 μm, in the case of Fig. A.1). For $\xi_{min} \geq \xi_{plane}$, we assume that the curvature has essentially no more influence on k_d, so that its value is given by Eq. (4) and it can be called $k_{d\text{-}plane}$. ξ_{plane} can be determined by equating Eq. (2) and Eq. (4) and solving for to ξ_{min} (=ξ_{plane}):

$$\xi_{plane} = \frac{\alpha}{2}\left(\frac{\alpha + \sqrt{\alpha^2 + 4D\beta}}{\beta^2}\right) + \frac{D}{\beta} \tag{A.11}$$

$$\alpha = 0.1 D^{\frac{2}{3}} \nu_f^{-\frac{1}{6}} \sqrt{\frac{4g(\rho_s - \rho_f)}{\eta_f}} R \qquad \beta = 0.207 D^{\frac{2}{3}} \nu_f^{-\frac{1}{6}} \sqrt{\frac{2g(\rho_s - \rho_f)}{\eta_f}} \sqrt{R} \tag{A.12}$$

Fig. A.1 also shows the trend of Eq. (A.11) for the above parameters (grey solid line, right vertical axis), and shows that the plane varies with R. For $R = 1$ μm, $\xi_{plane} \approx 130$ μm and its value decreases up to $R \approx 24$ μm when the ξ_{plane} is ≈ 48 μm. For higher values of R, ξ_{plane} increases monotonically.

In the absence of theoretical approaches to describe the dissolution of solid drugs from concave surfaces, we have adopted the following empirical equation:

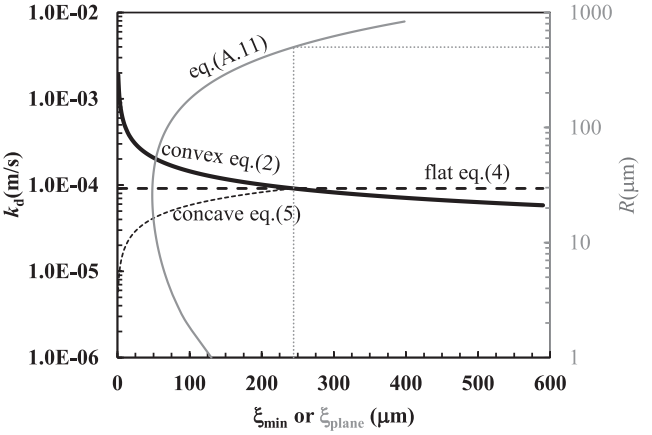

Fig. A.1. k_d dependence on the surface curvature radius ξ_{min} according to Eq. (2) (convex surfaces), Eq. (4), (flat surfaces) and Eq. (5) (concave surfaces assuming $n = 0.49$). All other parameters are: $D = 5{\cdot}10^{-10}$ m^2/s, $v_f = 10^{-6}$ m^2/s, $\eta_f = 10^{-3}$ Pa·s, $\rho_s = 1500$ kg/m^3 and $\rho_f = 1000$ kg/m^3) [10] and $R = 500$ μm. The dotted grey line helps distinguish the ξ_{plane} and the R values (eq. A.11) corresponding to the intersection between Eq. (2) and Eq. (4). For R between 1 and 840 μm, the intersection point moves on the solid grey line.

$$k_d = k_{d-plane}\left(\frac{\xi_{min}}{\xi_{plane}}\right)^n \tag{5}$$

where n is a power-law parameter. Basically, Eq. (5) (dashed thin line in Fig. A.1) assumes that, in contrast to convex surfaces, the dissolution kinetics decrease when the radius of curvature (ξ_{min}) of the concave surface becomes smaller because the relative velocity ((ΔU) between the surface and the fluid decreases locally. In summary, eqs. (2), (4), and (5) allow us to determine the correct k_d value when moving with continuity from convex to flat or concave to flat surfaces characterized by different radii of curvature (ξ_{min}).

Considering the definition of k_d (=D/δ), our approach implies that the thickness of BL on an irregular surface is position-dependent and, in the case of a convex surface, increases with ξ_{min} up to ξ_{plane}, where it assumes the thickness competing with a flat surface (plane). After that, it remains constant since the flat surface condition is satisfied. Conversely, in the case of a concave surface, it decreases with ξ_{min} starting from δ_{plane}.

Governing equations

The total mass balance of the drug states that the change over time in the mass of the drug in the bulk fluid phase (M_b) must be equal to the drug flux leaving the solid dissolving surface S:

$$\frac{dM_b}{dt} = V\frac{dC_b}{dt} = -S\left(D\frac{\partial C}{\partial \xi}\right)\Big|_{\xi=\xi_{max}} = SK(C_s - C_b) \tag{6}$$

where V is the bulk liquid volume (supposed constant) and K (m/s) is the *overall* mass transfer coefficient [32]:

$$K = \frac{\xi_{min}/\xi_{max}}{\frac{1}{k_d} + \frac{1}{k_m}\frac{\xi_{max}}{\xi_{min}}} \tag{7}$$

Since we are dealing with irregularly shaped particles, k_d and hence K are position dependent, and the description of the whole dissolution phenomenon requires a subdivision of S into elementary surfaces S_i (see Fig. 2), which are approximated by an osculating circle of radius $\xi_{min\text{-}i}$ such that:

$$S = \sum_i \Delta S_i \tag{A.13}$$

The evaluation of the drug mass M_b^i dissolved in the infinitesimal time dt from the elementary surface ΔS_i is thus given by:

$$\frac{dM_b^i}{dt} = -\frac{dM_s^i}{dt} = K(\xi_{min-i})\Delta S_i(C_s - C_b) \tag{A.14}$$

where M_s^i indicates the solid drug mass associated with ΔS_i. Consequently, we have:

$$\frac{dM_b}{dt} = V\frac{dC_b}{dt} = \sum_i \frac{dM_b^i}{dt} = (C_s - C_b)\sum_i K(\xi_{min-i})\Delta S_i \tag{A.15}$$

The change over time of the local surface radius of curvature $\xi_{min\text{-}i}$ can be evaluated using the following equation:

$$\frac{dM_s^i}{dt} = \rho_s \Delta S_i \frac{d\xi_{min-i}}{dt} = -K(\xi_{min-i})\Delta S_i(C_s - C_b) \qquad \frac{d\xi_{min-i}}{dt} = -\frac{K(\xi_{min-i})}{\rho_s}(C_s - C_b) \tag{A.16}$$

Typically, the C_s time variation induced by a surface phase transformation (polymorphic or amorphous– crystalline) is described by a first order reaction [51]:

$$C_s(t) = C_{sf} + (C_{s0} - C_{sf})e^{-k_r t} \tag{8}$$

where C_{sf} and C_{s0} are, respectively, the final and initial values of solubility while k_r is the recrystallization constant.

Actually, eqs.(A.14)-(A.16) hold as long as (and dissolution takes place until) $C_b < C_s$. When $C_b \geq C_s$, a recrystallization takes place in the bulk fluid. This is governed by Eq. (10):

$$\frac{dM_c}{dt} = -k_{rb}\, V(C_s(t) - C_b(t)) \qquad C_b(t) \geq C_s(t) \tag{10}$$

where M_c is the amount of recrystallized solid and k_{rb} is the bulk recrystallization rate. Obviously, the initial value for M_c is set to zero.

To evaluate C_b and close the balance between unknowns and equations, the total mass balance of the drug can be considered (Eq. (9)):

$$M_0 = \sum_i M_s^i + VC_b(t) + M_c(t) \tag{9}$$

By deriving Eq. (9) in time, we have:

$$0 = \sum_i \frac{dM_s^i}{dt} + V\frac{dC_b}{dt} + \frac{dM_c}{dt} \tag{A.17}$$

Combining eqs.(A.16), (A.17) and (10) we have:

$$V\frac{dC_b}{dt} + \frac{dM_c}{dt} = K(\xi_{min-i})\Delta S_i(C_s - C_b) \tag{A.18}$$

i.e.:

$$\frac{dC_b}{dt} = (C_s - C_b)\frac{\sum_i K(\xi_{min-i})\Delta S_i}{V} \qquad C_b(t) < C_s(t) \tag{A.19}$$

$$\frac{dC_b}{dt} = (C_s - C_b)k_{rb} \qquad C_b(t) \geq C_s(t) \tag{A.20}$$

Eqs. (A.19)-(A.20) make clear that C_b variation is due in part to dissolution (when $C_b(t) < C_s(t)$) and in part to recrystallization (when $C_b(t) > C_s(t)$).

Let us summarize the whole process described before. In the first phase, as long as $C_b(t) < C_s(t)$, the dissolution process takes place and C_b increases until $C_b(t) = C_s(t)$. The dissolution process is controlled by the following nonlinear ordinary differential system:

$$\frac{d\xi_{min-i}}{dt} = -\frac{K(\xi_{min-i})}{\rho_s}(C_s - C_b) \quad \forall i \quad C_b(t) < C_s(t) \tag{A.21}$$

$$\frac{dC_b}{dt} = (C_s - C_b)\frac{\sum_i K(\xi_{min-i})\Delta Si}{V} \quad C_b(t) < C_s(t) \tag{A.22}$$

and the following initial conditions are considered:

$$\xi_{min-i} = \xi^0_{min-i} \quad \forall_i \tag{A.23}$$

$$C_b(0) = 0 \tag{A.24}$$

$$M_c(0) = 0 \tag{A.25}$$

While Eq. (A.21) is used to determine the progressive change in particle volume and shape by evaluating the radii of curvature ξ_{min-i}, Eq. (A.22) allows us to determine the resulting increase in C_b. In the second phase, which finally occurs from time t^* when $C_b(t^*) = C_s(t^*)$, dissolution is stopped and recrystallization in the bulk fluid is the only phenomenon affecting C_b:

$$\frac{dC_b}{dt} = (C_s - C_b)k_{rb} \quad C_b(t) \geq C_s(t) \tag{A.26}$$

$$\frac{d\xi_{min-i}}{dt} = 0 \quad \forall i \quad C_b(t) \geq C_s(t) \tag{A.27}$$

$$\frac{dM_c}{dt} = -k_{rb}V(C_s(t) - C_b(t)) \quad C_b(t) \geq C_s(t) \tag{A.28}$$

Eq. (A.26) and (A.28) analytical solution reads:

$$C_b(t) = (C_{s0} - C_{sf})\frac{k_{rb}}{k_{rb} - k_r}\left(e^{-k_r t} - e^{-k_{rb}t}\right) + C_{sf}(1 - e^{-k_{rb}t}) \tag{A.29}$$

$$\frac{M_c(t)}{Vk_{rb}} = \frac{C_{s0} - C_{sf}}{k_r}\left(1 - \frac{k_{rb}}{k_{rb} - k_r}\right)e^{-k_r t} + \frac{k_{rb}C_{s0} - k_r C_{sf}}{(k_{rb} - k_r)k_{rb}}e^{-k_{rb}t} \tag{A.30}$$

References

[1] M. Grassi, G. Grassi, Application of mathematical modeling in sustained release delivery systems, Expert Opinion on Drug Delivery 11 (8) (2014) 1299–1321, https://doi.org/10.1517/17425247.2014.924497.

[2] J. Siepmann, F. Siepmann, Mathematical modelling of drug dissolution, Int. J. Pharm. 453 (2013) 12–24, https://doi.org/10.1016/j.ijpharm.2013.04.044.

[3] K.C. Kwan, Oral bioavailability and first pass effects, Drug Metab. Dispos. 5 (1997) 1329–1336.

[4] R. Naidu, K.T. Semple, M. Megharaj, A.L. Juhasz, N.S. Bolan, S.K. Gupta, B. E. Clothier, R. Schulin, Bioavailability: definition, assessment and implications for risk assessment, Dev. Soil Sci. 32 (2008) 39–51, https://doi.org/10.1016/S0166-2481(07)32003-5.

[5] G.L. Amidon, H. Lennernäs, V.P. Shah, J.R. Crison, A theoretical basis for a biopharmaceutics drug classification: the correlation of in vitro drug product dissolution and in vivo bioavailability, Pharm. Res. 12 (1995) 413–420, https://doi.org/10.1208/s12248-014-9620-9.

[6] T. Loftsson, M.E. Brewster, Pharmaceutical applications of cyclodextrins: basic science and product development, J. Pharm. Pharmacol. 62 (2010) 1607–1621, https://doi.org/10.1111/j.2042-7158.2010.01030.x.

[7] M. Davis, G. Walker, Recent strategies in spray drying for the enhanced bioavailability of poorly water-soluble drugs, J. Control. Release 269 (2018) 110–127, https://doi.org/10.1016/j.jconrel.2017.11.005.

[8] M.R. Gigliobianco, C. Casadidio, R. Censi, P. Di Martino, Nanocrystals of Poorly Soluble Drugs: Drug Bioavailability and Physicochemical Stability, Pharmaceutics 10 (134) (2018) 2–29, https://doi.org/10.3390/pharmaceutics10030134.

[9] S. Bertoni, B. Albertini, N. Passerini, Spray Congealing: An Emerging Technology to Prepare Solid Dispersions with Enhanced Oral Bioavailability of Poorly Water Soluble Drugs, Molecules 24 (3471) (2019) 1–21, https://doi.org/10.3390/molecules24193471.

[10] M. Grassi, G. Grassi, R. Lapasin, I. Colombo, Understanding Drug Release and Absorption Mechanisms: A Physical and Mathematical Approach, CRC Press, Boca Raton, USA, 2007.

[11] M. Grassi, I. Colombo, R. Lapasin, Drug release from an ensemble of swellable crosslinked polymer particles, J. Control. Release 68 (1) (2000) 97–113, https://doi.org/10.1016/S0168-3659(00)00241-8.

[12] D. Hasa, D. Voinovich, B. Perissutti, M. Grassi, A. Bonifacio, V. Sergo, C. Cepek, M. R. Chierotti, R. Gobetto, S. Dall'Acqua, S. Invernizzi, Enhanced Oral Bioavailability of Vinpocetine through Mechanochemical Salt Formation: Physico-Chemical Characterization and In Vivo Studies, Pharm. Res. 28 (8) (2011) 1870–1883, https://doi.org/10.1007/s11095-011-0415-8.

[13] Y. Tsume, D.M. Mudie, P. Langguth, G.E. Amidon, G.L. Amidon, The biopharmaceutics classification system: subclasses for in vivo predictive dissolution (IPD) methodology and IVINC, Eur. J. Pharm. Sci. 57 (2014) 152–163, https://doi.org/10.1016/j.ejps.2014.01.009.

[14] S. Baghel, H. Cathcart, N.J. O'Reilly, Polymeric amorphous solid dispersions: a review of amorphization, crystallization, stabilization, solid-state characterization, and aqueous solubilization of biopharmaceutical classification system class II drugs, Journal of Pharmaceutical Sciences 105 105 (9) (2016) 2527–2544, https://doi.org/10.1016/j.xphs.2015.10.008.

[15] S. Deshmukh, A. Avachat, A. Garka, N. Khurana, J.-M. Cardot, Optimization of a Dissolution Method in Early Development Based on IVIVC Using Small Animals: Application to a BCS Class II Drug, Dissolution Technol. 23 (4) (2016) 34–41.

[16] E.J. Kim, J.H. Kim, M.S. Kim, S.H. Jeong, D.H. Choi, Process Analytical Technology Tools for Monitoring Pharmaceutical Unit Operations: A Control Strategy for Continuous Process Verification, Pharmaceutics 13 13 (919) (2021) 2–45, https://doi.org/10.3390/pharmaceutics13060919.

[17] https://www.ema.europa.eu/en/ich-q8-r2-pharmaceutical-development accessed August 5th 2021.

[18] Manca D., Ed. Computer Aided Chemical Engineering Quantitative Systems Pharmacology Models and Model-Based Systems with Applications Volume 42. 2018, Elsevier B.V., Amsterdam.

[19] R. Laitinen, J. Lahtinen, P. Silfsten, E. Vartiainen, P. Jarho, J. Ketolainen, An optical method for continuous monitoring of the dissolution rate of pharmaceutical powders, J. Pharm. Biomed. Anal. 52 (2) (2010) 181–189, https://doi.org/10.1016/j.jpba.2010.01.011.

[20] J.J. Sheng, P.J. Sirois, J.B. Dressman, G.L. Amidon, Particle diffusional layer thickness in a USP dissolution apparatus II: a combined function of particle size and

paddle speed, J. Pharm. Sci. 97 (11) (2008) 4815–4829, https://doi.org/10.1002/jps.21345.
[21] A.W. Hixson, J.H. Crowell, Dependence of reaction velocity upon surface and agitation I, Theoretical consideration. Industrial and Engineering Chemistry 23 (8) (1931) 923–931, https://doi.org/10.1021/ie50260a018.
[22] A.W. Hixson, J.H. Crowell, Dependence of reaction velocity upon surface and agitation II. Experimental procedure in study surface, Ind. Eng. Chem. 23 (9) (1931) 1002–1009, https://doi.org/10.1021/ie50261a009.
[23] A.W. Hixson, J.H. Crowell, Dependence of reaction velocity upon surface and agitation III. Experimental procedure in study of agitation, Ind. Eng. Chem. 23 (10) (1931) 1160–1168, https://doi.org/10.1021/ie50262a025.
[24] P.V. Pedersen, K.F. Brown, Dissolution profile in relation to initial particle distribution, Journal of Pharmaceutical Science 64 (7) (1975) 1192–1195, https://doi.org/10.1002/jps.2600640713.
[25] P.V. Pedersen, K.F. Brown, Size distribution effects in multiparticulate dissolution, Journal of Pharmaceutical Science 64 (12) (1975) 1981–1986, https://doi.org/10.1002/jps.2600641217.
[26] P.V. Pedersen, K.F. Brown, General class of multiparticulate dissolution models, Journal of Pharmaceutical Science 66 (10) (1977) 1435–1438, https://doi.org/10.1002/jps.2600661022.
[27] P.V. Pedersen, J.W. Myrick, Versatile kinetic approach to analysis of dissolution data, Journal of Pharmaceutical Science 67 (10) (1978) 1450–1455, https://doi.org/10.1002/jps.2600671034.
[28] J.P. Hsu, B.T. Liu, Dissolution of solid particles in liquids: a reaction-diffusion model, Colloids Surf. 69 (4) (1993) 229–238, https://doi.org/10.1016/0166-6622(93)80004-Y.
[29] A. Dokoumetzidis, V. Papadopoulou, G. Valsami, P. Macheras, Development of a reaction-limited model of dissolution: Application to official dissolution tests experiments, Int. J. Pharm. 355 (1-2) (2008) 114–125, https://doi.org/10.1016/j.ijpharm.2007.11.056.
[30] B. Shekunov, E.R. Montgomery, Theoretical analysis of Drug dissolution: I. Solubility and intrinsic dissolution rate, Journal of Pharnaceutical Sciences 105 105 (9) (2016) 2685–2697, https://doi.org/10.1016/j.xphs.2015.12.006.
[31] N. Guo, B. Hou, N.a. Wang, Y. Xiao, J. Huang, Y. Guo, S. Zong, H. Hao, In situ monitoring and modeling of the solution-mediated polymorphic transformation of rifampicin: from form II to form I, Journal of Pharmaceutical Sciences 107 107 (1) (2018) 344–352, https://doi.org/10.1016/j.xphs.2017.10.004.
[32] M. Abrami, L. Grassi, R. di Vittorio, D. Hasa, B. Perissutti, D. Voinovich, G. Grassi, I. Colombo, M. Grassi, Dissolution of an ensemble of differently shaped polydispersed drug particles undergoing solubility reduction: mathematical modelling, ADMET & DMPK 8 (2020) 297–313, https://doi.org/10.5599/admet.841.
[33] J.P. Hsu, D.L. Lin, M.J. Lin, Dissolution of solid particles in liquids: a surface layer model, Colloids Surf. 61 (1991) 35–47, https://doi.org/10.1016/0166-6622(91)80297-2.
[34] J. Wang, D.R. Flanagan, General solution for diffusion controlled dissolution of spherical particles 1, Theory. Journal of Pharmaceutical Sciences 88 (7) (1999) 731–738, https://doi.org/10.1021/js980236p.
[35] D. Hasa, B. Perissutti, D. Voinovich, M. Abrami, R. Farra, S.M. Fiorentino, G. Grassi, M. Grassi, Drug Nanocrystals: Theoretical Background of Solubility Increase and Dissolution Rate Enhancement, Chem. Biochem. Eng. Q. 28 (2014) 247–258. https://doi.org/10.15255/CABEQ.2013.1835.
[36] J. Wang, D.R. Flanagan, General solution for diffusion controlled dissolution of spherical particles 2. Evaluation of experimental data, J. Pharm. Sci. 91 (2) (2002) 534–542, https://doi.org/10.1002/jps.10039.
[37] D.M. D'Arcy, T. Persoons, Mechanistic Modelling and Mechanistic Monitoring: Simulation and Shadowgraph Imaging of Particulate Dissolution in the Flow-Through Apparatus, J. Pharm. Sci. 100 (3) (2011) 1102–1115, https://doi.org/10.1002/jps.22337.
[38] D.M. D'Arcy, T. Persoons, Understanding the Potential for Dissolution Simulation to Explore the Effects of Medium Viscosity on Particulate Dissolution, AAPS PharmSciTech 20 (47) (2019) 2–13, https://doi.org/10.1208/s12249-018-1260-4.
[39] U. Thormann, M. De Mieri, M. Neuburger, S. Verjee, P. Altmann, M. Hamburger, G. Imanidis, Mechanism of chemical degradation and determination of solubility by kinetic modeling of the highly unstable sesquiterpene lactone nobilin in different media, J. Pharm. Sci. 103 (10) (2014) 3139–3152, https://doi.org/10.1002/jps.24100.
[40] M. Mosharraf, C. Nyström, The effect of particle size and shape on the surface specific dissolution rate of micronized practically insoluble drugs, Int. J. Pharm. 122 (1995) 35–47, https://doi.org/10.1016/0378-5173(95)00033-F.
[41] D. Hirai, Y. Iwao, S.I. Kimura, S. Noguchi, S. Itai, Mathematical model to analyze the dissolution behaviour of metastable crystals or amorphous drug accompanied with solid-liquid interface reaction, Int. J. Pharm. 522 (2017) 58–65, https://doi.org/10.1016/j.ijpharm.2017.02.050.
[42] Q. Yuan, X. Jia, R.A. Williams, Validation of a multi-component digital dissolution model for irregular particles, Powder Technol. 240 (2013) 25–30, https://doi.org/10.1016/j.powtec.2012.07.011.
[43] R.C. Snyder, S. Veesler, M.F. Doherty, The Evolution of Crystal Shape During Dissolution: Predictions and Experiments, Cryst. Growth Des. 8 (4) (2008) 1100–1101, https://doi.org/10.1021/cg7008495.
[44] H. Heywood, Particle shape coefficients, J. Imp. Coll. Chem. Eng. Soc. 8 (1954) 25–33.
[45] A. Parmar, S. Sharma, Engineering design and mechanistic mathematical models: standpoint on cutting edge drug delivery, Trends Anal. Chem. 100 (2018) 15–35, https://doi.org/10.1016/j.trac.2017.12.008.
[46] G. Chiarappa, A. Piccolo, I. Colombo, D. Hasa, D. Voinovich, M. Moneghini, G. Grassi, R. Farra, M. Abrami, P. Posocco, S. Pricl, M. Grassi, Exploring the Shape Influence on Melting Temperature, Enthalpy, and Solubility of Organic Drug Nanocrystals by a Thermodynamic Model, Crystal Growth Design 17 (8) (2017) 4072–4083, https://doi.org/10.1021/acs.cgd.6b01714.
[47] J.Y.Y. Heng, A. Bismarck, A.F. Lee, K. Wilson, D.R. Williams, Anisotropic Surface Energetics and Wettability of Macroscopic Form I Paracetamol Crystals, Langmuir 22 (2006) 2760–2769.
[48] W.E. Ranz, W.R. Marshall, Evaporation from drops. 1, Chem. Eng. Prog. 48 (1952) 141–146.
[49] W.E. Ranz, W.R. Marshall, Evaporation from drops. 2, Chem. Eng. Prog. 48 (1952) 173–180.
[50] V.G. Levich, Physicochemical Hydrodynamics, Prentice Hall, Englewood Cliffs, N. J., 1962, pp. 60–72.
[51] H. Nogami, T. Nagai, T. Yotsuyanagi, Dissolution phenomena of organic medicinals involving simultaneous phase changes, Chemical Pharmaceutical Bulletin 17 (3) (1969) 499–509, https://doi.org/10.1248/cpb.17.499.
[52] P.J. Skrdla, P.D. Floyd, P.C. Dell'Orco, Modeling recrystallization kinetics following the dissolution of amorphous drugs, Mol. Pharmaceutics 17 (1) (2020) 219–228, https://doi.org/10.1021/acs.molpharmaceut.9b00940.
[53] N.A. Mitchell, P.J. Frawley, Nucleation kinetics of paracetamol–ethanol solutions from metastable zone widths, J. Cryst. Growth 312 (19) (2010) 2740–2746, https://doi.org/10.1016/j.jcrysgro.2010.05.043.
[54] H. J. Motulsky, A. Christopoulos. Fitting models to biological data using linear and non linear regression. A practical guide to curve fitting. 2003. GraphPad Software Inc., San Diego, USA. www.graphpad.com.
[55] J.K. Mitchell, K. Soga, Fundamental of soil behavior, John Wiley & Sons, 2005.
[56] E. Berrezueta, J. Cuervas-Mons, A. Rodríguez-Rey, B. Ordóñez-Casado, Representativity of 2D Shape Parameters for Mineral Particles in Quantitative Petrography, Minerals 9 (768) (2019) 1–21, https://doi.org/10.3390/min9120768.
[57] H. Wadell, Volume, Shape, and Roundness of Rock particles, J. Geol. 40 (1932) 443–451.
[58] J. Zheng, R.D. Hryciw, Traditional soil particle sphericity, roundness and surface roughness by computational geometry, Géotechnique 65 (6) (2015) 494–506, https://doi.org/10.1680/geot.14.P.192.
[59] J.H. de Smidt, J.G. Fokkens, H. Grijseels, D.J.A. Crommelin, Dissolution of theophylline monohydrate and anhydrous theophylline in buffer solutions, Journal of Pharmaceutical Science 75 (5) (1986) 497–501, https://doi.org/10.1002/jps.2600750515.
[60] S. Tseng, T.H. Lin, J.P. Hsu, Unsteady dissolution of particle of various shapes in a stagnant liquid, Chem. Eng. Sci. 123 (2015) 573–578, https://doi.org/10.1016/j.ces.2014.11.023.
[61] R.C. Tolman, The effect of droplet size on surface tension, J. Chem. Phys. 17 (3) (1949) 333–337, https://doi.org/10.1063/1.1747247.
[62] V.M. Samsonov, N.Y. Sdobnyakov, A.N. Bazulev, Size dependence of the surface tension and the problem of Gibbs thermodynamics extension to nanosystems, Colloid Surf. A. 239 (1-3) (2004) 113–117, https://doi.org/10.1016/j.colsurfa.2004.01.016.
[63] J.S. Rowlinson, B. Windom, Molecular Theory of Capillarity, Clarendon Press, Oxford, 1982.